Supplement of Atmos. Chem. Phys., 23, 7461–7477, 2023
https://doi.org/10.5194/acp-23-7461-2023-supplement

Atmospheric Chemistry and Physics
Open Access

Supplement of

Chemical evolution of primary and secondary biomass burning aerosols during daytime and nighttime

Amir Yazdani et al.

Correspondence to: Satoshi Takahama (satoshi.takahama@epfl.ch) and Athanasios Nenes (athanasios.nenes@epfl.ch)

S1 Size distribution of bbOA

Figure S1a shows the decrease in the OA concentration in a reference experiment (experiment 1). A first-order wall loss can explain the trend of the OA concentration well ($R^2 = 0.8$). The size distribution of OA averaged from -2 to 2 h is shown in Figure S1b. The distribution has its mode close to 200 nm for this experiment and for the majority of other experiments of this study.

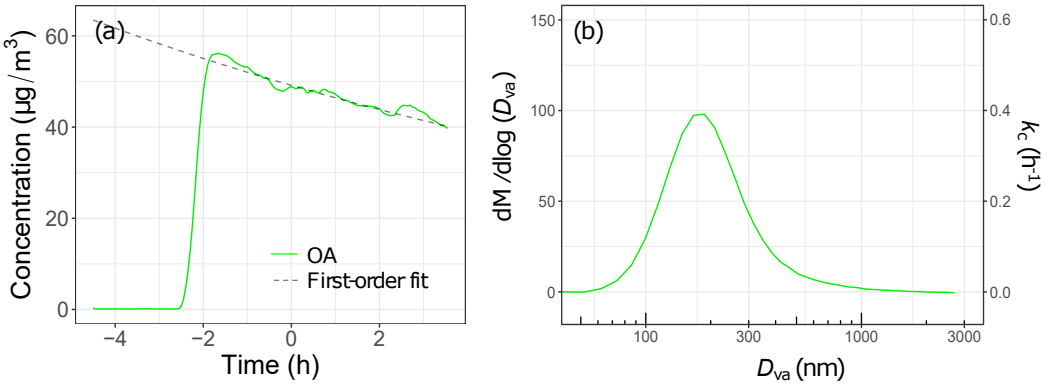

Figure S1. (a) The AMS OA concentration and the first-order fit for Exp. 1 (reference). Injection of biomass burning emissions happens at -2 h. (b) The AMS size-resolved organic mass. The results are based on particle time-of-flight (PToF) data averaged from -2 to 2 h.

S2 Investigating the volatility of lignin-like compounds

In order to qualitatively rank the volatility of different species responsible for marker fragments, we interpreted thermodenuder measurements with a simplified model for a separate reference experiment (Florou et al., *in review*, 2023). This reference experiment is different from those those discussed in the main text. The thermodenuder design and operation is described by Gkatzelis et al. (2016) and Florou et al. (*in review*, 2023). The heating section is 50 cm in length with outer and inner diameters of 10 and 3.64 cm, respectively (the annulus is filled with sand to distribute the heat). The flow rate is 1 Lpm and the temperature profile is described by Wehner et al. (2002) and Lee et al. (2010) for similar systems. The centerline residence time was 16s at 298K (overall 32 s) in the heating section, with a residence time of 30s in the cooling section (cooled by convection).

Detailed (dynamic) modeling of the thermodenuder is described by Florou et al. (*in review*, 2023), but in this work we use a simplified approximation neglecting thermophoresis and assuming thermodynamic equilibrium at all temperatures, following the equation below:

$$A_i(T) = \frac{G_i(T) + A_i(T)}{1 + C_i^\star(T)/M(T)}, \tag{S1}$$

where $A_i(T)$ and $G_i(T)$ are aerosol-phase and gas-phase concentrations of the fragment i at temperature, T and $M(T)$ denotes the total organic mass. The sum of $A_i(T)$ and $G_i(T)$ are assumed to be the same between the bypass line and the thermodenuder line. The Clausius-Clapeyron equation was used to relate the saturations concentration, $C_i^\star$, at different temperatures:

$$C_i^\star(T) = \frac{298}{T}\, C_i^\star(298)\, \exp\left(\frac{\Delta H_v}{R}\left(\frac{1}{T} - \frac{1}{298}\right)\right). \tag{S2}$$

The total organic concentration has been assumed to be the value estimated by AMS considering a CE of unity. ΔH_v is assumed to be equal to 77 $\mathrm{kJ\,mol^{-1}}$ (Florou et al., *in review*, 2023). The Levenberg-Marquardt nonlinear least-Squares algorithm was used to find the optimum $C^\star$ for different marker fragments. For $C_2H_4O_2^+$, $C_9H_{11}O_3^+$, $C_{10}H_{13}O_3^+$, CO_2^+, and $C_4H_9^+$, the $C^\star(298)$ was estimated to span one order of magnitude: 1.09, 0.3, 0.22, 0.51, and 0.1 $\mu\mathrm{g\,m^{-3}}$, respectively. Due to simplifying assumptions (e.g., omission of thermophoresis or equilibrium state) these values should be considered approximate. Changing the enthalpy changes the absolute values, but C*s retain similar ratios, which is sufficient for our qualitative comparison.

According to this analysis, the $C_2H_4O_2^+$ is produced by the most volatile species (levoglucosan, anhydrosugars) and the CO_2^+ by the least volatile ones. As can be seen from Fig. S3, a lower loss rate is observed for $C_9H_{11}O_3^+$ in the absence of oxidants compared to other fragments including $C_2H_4O_2^+$. This suggests a lower volatility of the corresponding species, as their concentration is mainly affected by particle-phase wall losses compared to particle- and gas-phase wall losses for levoglucosan. This phenomenon is observed in all experiments before the injection of oxidants.

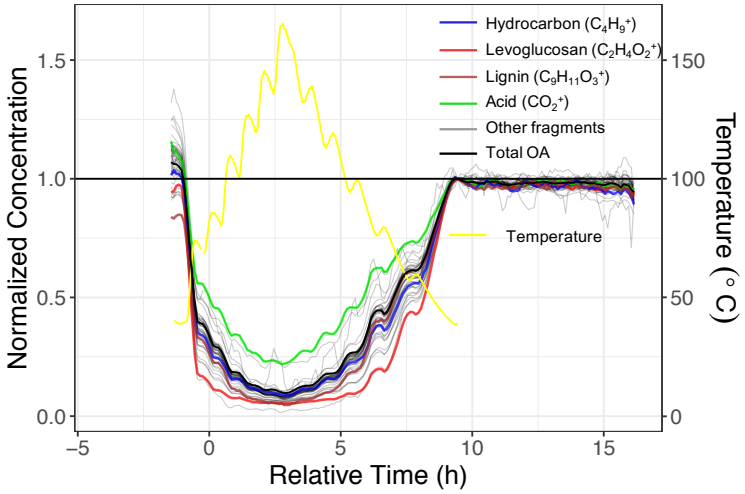

Figure S2. Concentration time series of individual AMS fragments after passing chamber OA through a thermodenuder (normalized by the concentrations through the bypass line). The temperature of the thermodenuder is shown in yellow.

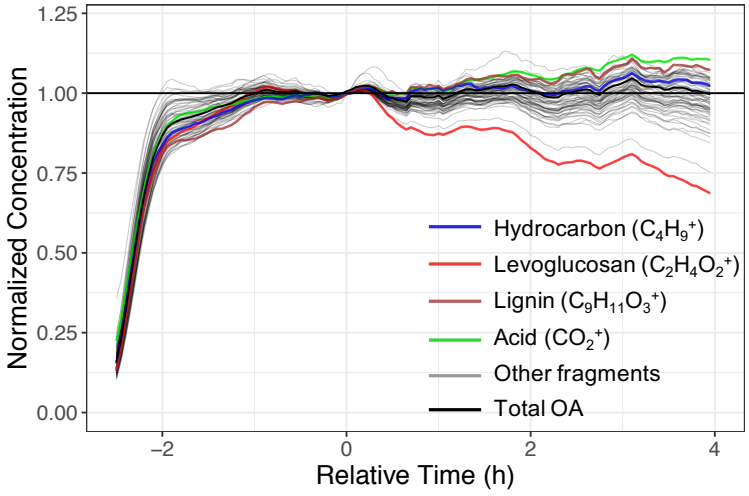

Figure S3. Time series of normalized concentrations of AMS fragments in a reference experiment (Exp. 3).

S3 AMS and FTIR comparison

OA concentrations estimated using FTIR and AMS are correlated ($R^2 = 0.75$; Fig. S4). Aging with UV increases the OM:OC ratio more than aging with the nitrate radical. We also observe that the general increase in OM:OC with aging is captured by both methods (Fig. S4c). However, the absolute values are different. PTFE filters that belong to each experiment (primary and aged in order) are as follows: Exp. 1 (filters F1, F2), Exp. 2 (F9, 10), Exp. 3 (F16, 17), Exp. 4 (F18, 19), Exp. 5 (F20, 21), Exp. 6 (F4, 5), Exp. 7 (F11, 12), Exp. 8 (F6, 7), and Exp. (F13, 14). F3, 8, and 18 were blank filters put in the chamber for a few minutes. Reported AMS OA is averaged over filter sampling period and not corrected for the collection efficiency (CE).

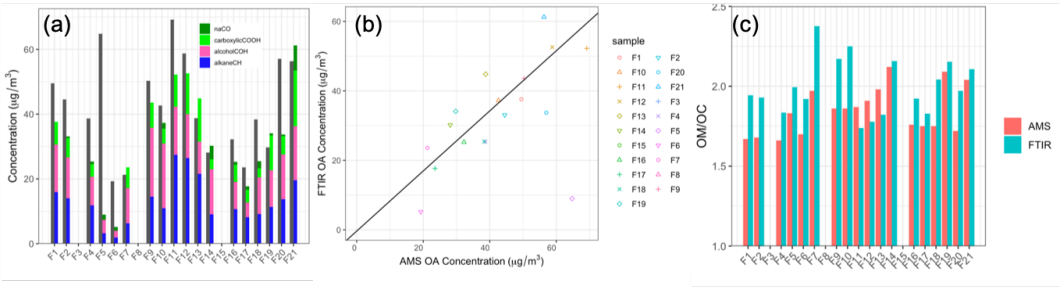

Figure S4. The OA mass concentration measured with FTIR (functional groups are color codded) and AMS (averaged over the filter sampling periods) (a). Scatter plot comparing OA concentrations measured by AMS and FTIR (b). OM:OC ratios measured by AMS and FTIR (c).

S4 Dimension reduction of AMS mass spectra

In the figure below, the loadings of the first three principal components (up to m/z 73) for an uncentered PCA on the AMS spectra of the chamber experiments are shown. The first PC has high negative loadings of oxygenated fragments ions such as CO^+, CO_2^+, CHO^+, and $C_2H_3O^+$, showing the direction of aging. The CHO^+ fragment has a high positive loading and CO^+ and CO_2^+ have high negative loadings for PC2, suggesting that this PC distinguishes between carboxylic and dicarboxylic acids which are detected by CO_2^+ and alcohols which produce strong signals of CHO^+. This is supported by FTIR spectra of pellet burning samples which have higher PC2 scores than and strong signatures of the alcohol group than their wood burning counterparts. PC3 has high positive loadings of CO^+ and CO_2^+ and high negative loadings of $C_2H_4O_2^+$, showing the degradation of anhydrosugars with aging.

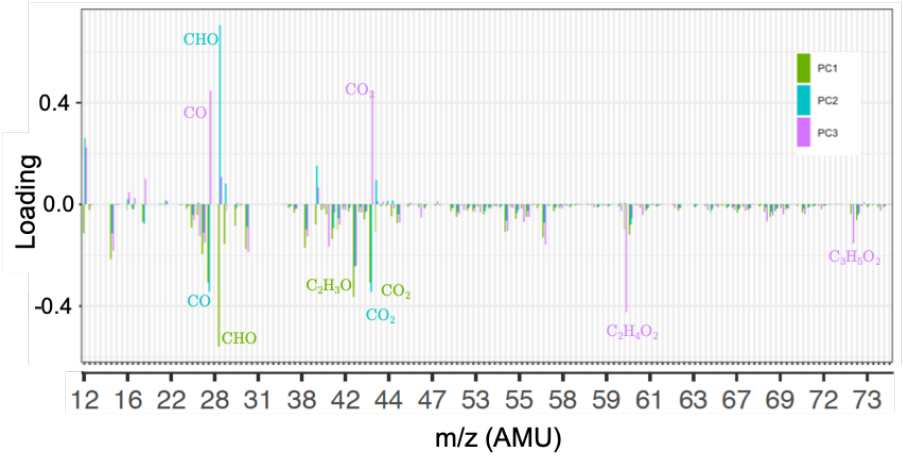

Figure S5. Loadings of the first three PCs.

S5 Ammonium-subtracted spectra

In the figure below ammonium-subtracted residual spectra are shown. A reference ammonium spectrum multiplied by a scaling factor, defined as the minimum ratio of each sample spectrum and reference ammonium spectrum, subtracted from the sample spectrum. CH peaks have been subtracted because there are CH peaks in the ammonium spectrum used for subtraction. Carboxylic acid and alcohol absorbances are clearly observed in these spectra.

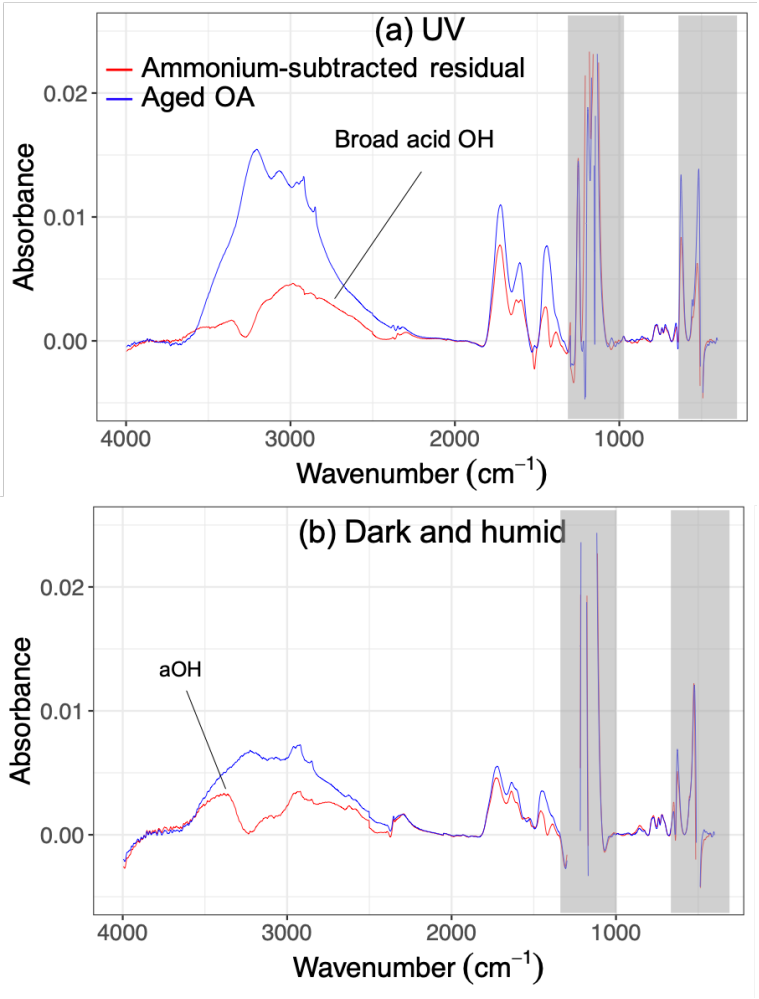

Figure S6. Ammonium-subtracted residual FTIR spectra of wood burning OA aged with UV (a) and nitrate radical (b) (Exp. 4, and 8, respectively).

S6 The FTIR spectrum of atmospheric smoke impacted $PM_{2.5}$

An example of atmospheric smoke impacted $PM_{2.5}$ samples (prescribed burning in the eastern US in 2013, validated by satellite observations; Yazdani, 2022). High organic loading, strong acid signatures, and very weak levoglucosan and invisible lignin-like signatures are observed in the Fig. S7. Compared to primary WB aerosols in chamber, weak levoglucosan and lignin peaks in this sample are observed in the ambient spectrum. On the other hand, the broad peak from 2400–3400 cm^{-1} suggests the high abundance of carboxylic acids, which are also observed in the WB residual spectra of S6a. This observation suggest the dominant contribution of wood burning (secondary aerosols) in this atmospheric sample although primary marker are quite weak.

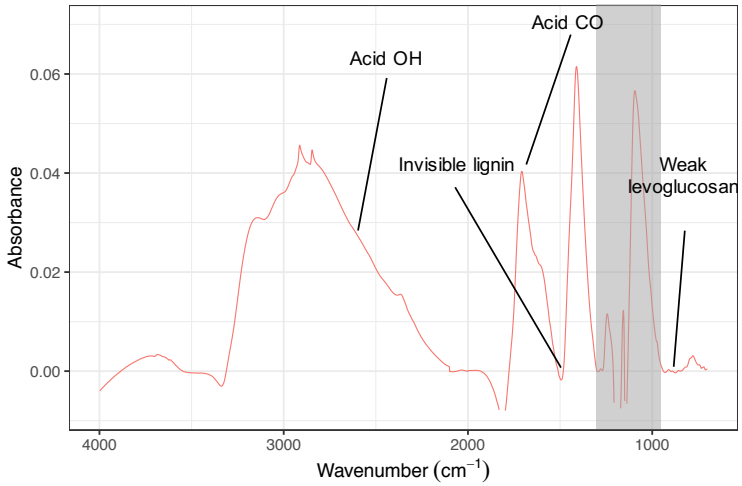

Figure S7. The FTIR spectrum of an atmospheric smoke-impacted $PM_{2.5}$ sample.

S7 Loss rates of different fragments

Based on the loss profiles for different fragments within two hours after the initiation of aging (when UV lights are on), the loss rates are estimated to be 0.38, 0.70, 0.24, and 0.23 h^{-1} for $C_2H_4O_2^+$, $C_9H_{11}O_3^+$, $C_{10}H_{13}O_3^+$, and $C_4H_9^+$.

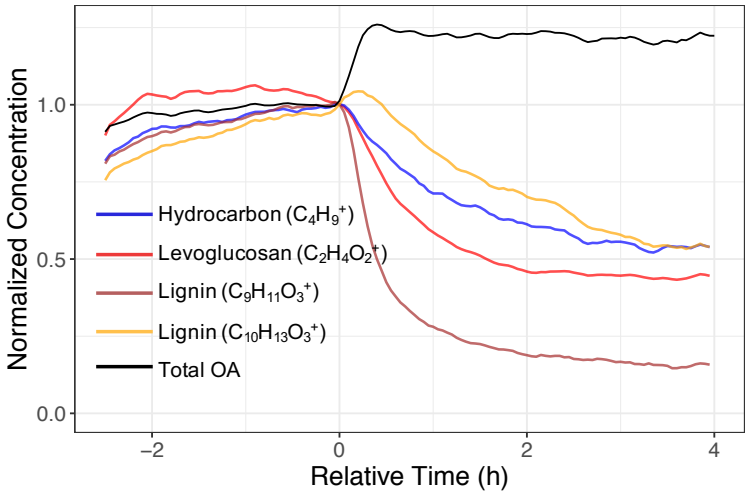

Figure S8. Smoothed time series of AMS OA concentration, and different tracer fragments in a UV experiment (Exp. 4).

S8 f_{44}:f_{43} ratios in residual spectra

In Fig. S9 the wall-loss corrected OA was calculated base on

$$C_{\mathrm{OA}}^{\mathrm{cor}}(t) = C_{\mathrm{OA}}^{\mathrm{obs}}(t) + k_{\mathrm{OA}} \int_{t_0}^{t} C_{\mathrm{OA}}^{\mathrm{obs}}(t)\, dt, \tag{S3}$$

where $C_{\mathrm{OA}}^{\mathrm{obs}}(t)$ is the observed (measured) OA concentration at time t, $C_{\mathrm{OA}}^{\mathrm{cor}}(t)$ is the wall-loss-corrected OA at the t, k_{OA} is the first-order wall loss rate based on the AMS OA. OC was calculated from the sum of C concentration for all fragments. Dividing OA time series by OM:OC time series gives a similar trend with different absolute values.

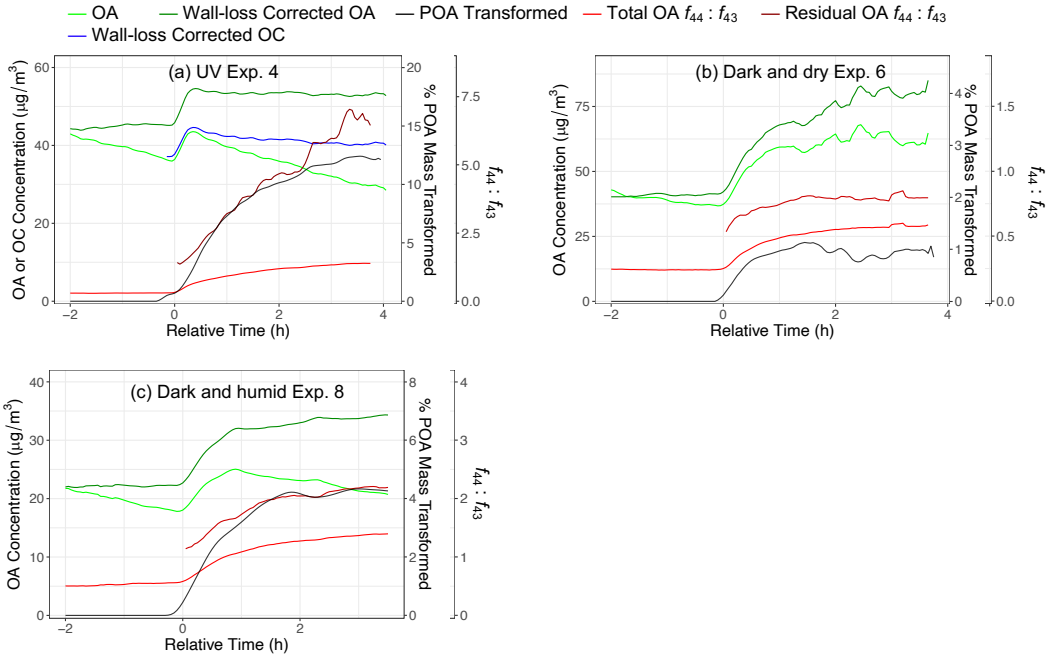

Figure S9. Time series of OA, OC concentrations, percentage of POA mass aged, and f_{44}:f_{43} for wood burning emissions in different aging scenarios.

As can be seen from Fig. S9, the trends of POA aging and f_{44}:f_{43} are similar in different experiments. The decrease in the OC concentration in the UV experiment with aging suggests the importance of other aging mechanisms such as photolysis in addition to the SOA condensation.

References

Gkatzelis, G. I., Papanastasiou, D. K., Florou, K., Kaltsonoudis, C., Louvaris, E., and Pandis, S. N.: Measurement of nonvolatile particle number size distribution, Atmospheric Measurement Techniques, 9, 103–114, https://doi.org/10.5194/amt-9-103-2016, 2016.

Lee, B. H., Kostenidou, E., Hildebrandt, L., Riipinen, I., Engelhart, G. J., Mohr, C., DeCarlo, P. F., Mihalopoulos, N., Prevot, A. S. H., Baltensperger, U., and Pandis, S. N.: Measurement of the ambient organic aerosol volatility distribution: application during the Finokalia Aerosol Measurement Experiment (FAME-2008), Atmospheric Chemistry and Physics, 10, 12 149–12 160, https://doi.org/10.5194/acp-10-12149-2010, publisher: Copernicus GmbH, 2010.

Wehner, B., Philippin, S., and Wiedensohler, A.: Design and calibration of a thermodenuder with an improved heating unit to measure the size-dependent volatile fraction of aerosol particles, Journal of Aerosol Science, 33, 1087–1093, https://doi.org/10.1016/S0021-8502(02)00056-3, 2002.

Yazdani, A.: Chemical characterization of organic aerosols with a focus on biomass burning and mid-infrared spectroscopy, Ph.D. thesis, École Polytechnique Fédérale de Lausanne, 2022.